Heliyon 11 (2025) e42598

Contents lists available at ScienceDirect

Heliyon

journal homepage: www.cell.com/heliyon

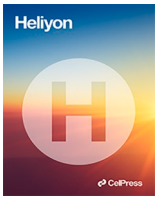

Research article

# Tissue-specified reconstruction modeling of the head and neck structure and its application in simulating airway obstruction

Huahui Xiong [a,b], Hui Tong [a,b], Yuhang Tian [a,b], Changjin Ji [a,b], Xiaoqing Huang [a,b], Yaqi Huang [a,b,*]

[a] School of Biomedical Engineering, Capital Medical University, Beijing, China
[b] Beijing Key Laboratory of Fundamental Research on Biomechanics in Clinical Application, Capital Medical University, Beijing, China

ARTICLE INFO

*Keywords:*
MRI images
Three-dimensional reconstruction
Registration
Finite element analysis

ABSTRACT

*Background and objective:* Three-dimensional (3D) reconstruction of head and neck tissues has extensive clinical applications, but due to the complexity and variability of tissue structure, there is still a lack of a complete scheme to reconstruct the head and neck tissues. This study aims to establish a tissue-specified multi-directional cross-sectional image sequence construction method to capture diverse tissue contour information,

*Methods:* The image sequences that are most conducive to acquiring the boundary contours of the target tissue are constructed from 3D MRI images of the head and neck in a non-traditional way based on the characteristics of each target tissue, and an effective registration strategy is used to integrate the boundaries of the target tissue segmented from multiple image sequences. The NURBS (Non-Uniform Rational B-Splines) surface modeling method is used to construct the 3D structure of the head and neck based on the segmented tissue boundaries, and then the constructed structure is used to build a fluid-structure interaction model to simulate airway collapse.

*Results:* The multi-directional cross-sectional image sequences of head and neck tissues were reconstructed, which successfully supplemented the missing boundary information in unidirectional image sequences commonly used in anatomical reconstructions. The boundaries of the tongue and soft palate were obtained from three corresponding sequential images respectively, and nonlinear registration methods were developed to match the intersections of the target tissue boundaries segmented from different image sequences. The complete 3D head and neck structure, including the surrounding tissues of the upper airway, was accurately reconstructed, and then directly converted into a finite element model through a meshing procedure. The head and neck numerical models successfully simulate airway collapse in both the obstructive sleep apnea patient and the normal subject, providing detailed information on soft tissue deformation and predicting the values of the airway critical closing pressure.

*Conclusions:* A complete 3D reconstruction scheme from multi-directional image sequence construction to nonlinear boundary registration and NURBS surface generation is established. The constructed model can accurately reflect the characteristics of real anatomical structure, and can be directly used for complex numerical simulations of upper airway collapse.

* Corresponding author.
*E-mail address:* yqhuang@ccmu.edu.cn (Y. Huang).

https://doi.org/10.1016/j.heliyon.2025.e42598
Received 22 September 2024; Received in revised form 25 January 2025; Accepted 9 February 2025
Available online 10 February 2025

## 1. Introduction

Three-dimensional (3D) reconstruction of human tissues is of great significance for clinical applications and research, such as surgical navigation, virtual surgery, tissue reconstruction, notably, the widely utilized biomechanical simulation analysis [1–5]. For example, some geometrically simplified numerical models of airway collapse have been applied to surgical planning and treatment outcome prediction for obstructive sleep apnea (OSA) [6–8]. These applications urgently need powerful 3D modeling technology to deal with complex human tissues. The construction of the head and neck 3D model has an important impact on the research of physiological functions such as breathing, speech and swallowing [9–13]. 3D MRI adopts 3D spatial encoding technology, and the image signal acquisition comes from volume excitation, which effectively reduces the adverse effect of the slice spacing of 2D MRI on the spatial resolution of the image, and is conducive to image reconstruction in other directions than the direction of image shooting. However, the human head and neck contain numerous tissues and organs with complex anatomical structures, which pose a serious challenge to the construction of 3D models based on medical images [14,15]. Although some 3D models have been constructed for the partial structure of the head and neck in specific studies, such as the tongue and soft palate [16–20], there is still a lack of a unified scheme for the construction of head and neck tissues.

Computer Aided Design (CAD) technology is widely used in industrial fields, such as the shape design of automobiles, ships, and aircrafts, as well as in the medical field [21,22]. Different from the standard parts design in industry, the human tissue morphology is complex and individual differences are large. This challenges the direct application of CAD technology in 3D modeling of human anatomy, highlighting the urgent need to develop a CAD approach specifically suited for modeling human tissues [23,24]. CAD modeling is based on powerful spline curve and surface technology, as well as flexible Boolean operations [25], which can provide technical support for complex human tissue modeling.

Unlike voxel-based modeling, CAD modeling essentially utilizes boundary curves to generate geometrical structures [26]. However, conventional unidirectional axial, sagittal, or coronal images restrict the boundary curve of the target tissue to a fixed orientation plane. This limitation makes it challenging to capture boundary details in other orientations, introducing uncertainties into the model. The problem is especially pronounced when the curvature of the tissue boundary varies significantly, as accurate modeling requires boundary information from multiple directions. Given the substantial morphological differences among various tissues, it is essential to develop imaging techniques that provide cross-sectional views in multiple orientations to better capture the geometry of each specific tissue in the head and neck region.

Another key challenge is aligning boundary information from different orientations. In our previous studies, we employed a linear registration method to align curves from parallel planes, but this approach is inadequate for multi-directional imaging [27]. The boundaries segmented from two intersecting images of the same tissue should intersect. Due to the partial volume effects and errors in the image reconstruction process, this basic property that should exist is destroyed.

Aiming at the problems mentioned above, the objective of this article is to establish a multi-directional image reconstruction and

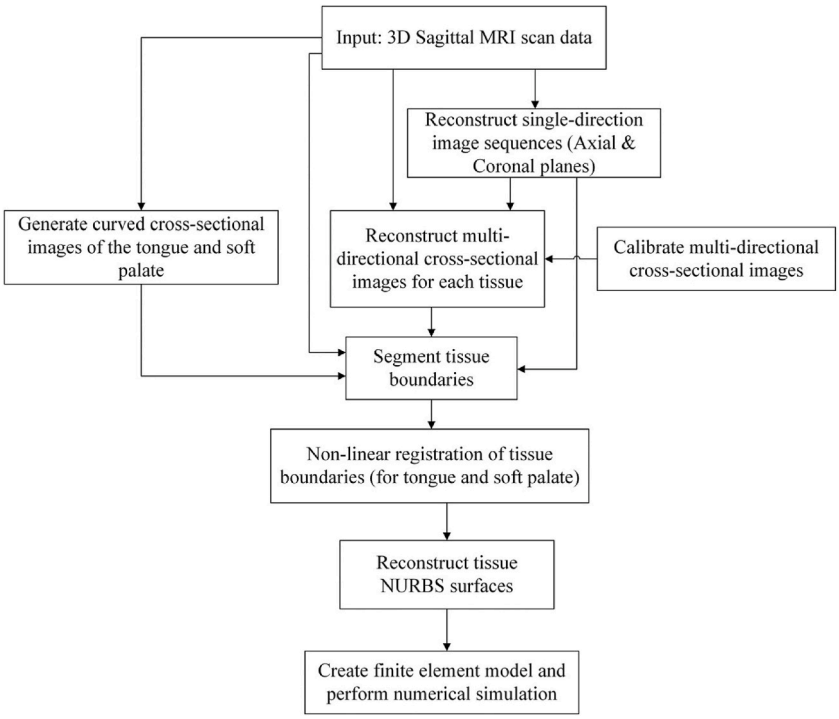


**Fig. 1.** Flowchart for tissue 3D reconstruction and numerical simulation.

nonlinear registration method based on 3D MRI images of the head and neck to build realistic 3D structures around the upper airway. Then, the 3D head and neck models were used to simulate the collapse of the upper airway.

## 2. Methods

3D MRI scans of the entire head and neck were conducted in a healthy subject and a patient with obstructive sleep apnea, both in a supine position. The raw 3D image was reconstructed into sagittal sequences, and the slice spacing was consistent with the pixel size, i.e., 0.67 mm. Based on such a sagittal sequence image the structures of head and neck tissues were reconstructed. This study was approved by the Ethics Committee of Capital Medical University, Beijing, China. The participant signed the informed consent prior to participation.

Fig. 1 is a flowchart of the specific steps for constructing the 3D structure of head and neck tissues in this study.

### 2.1. Reconstruction of multi-directional cross-sectional images

Due to the complexity of the head and neck structure, employing conventional boundary segmentation based on parallel two-dimensional series of images in the axial, coronal, or sagittal planes for three-dimensional structure reconstruction of a specific

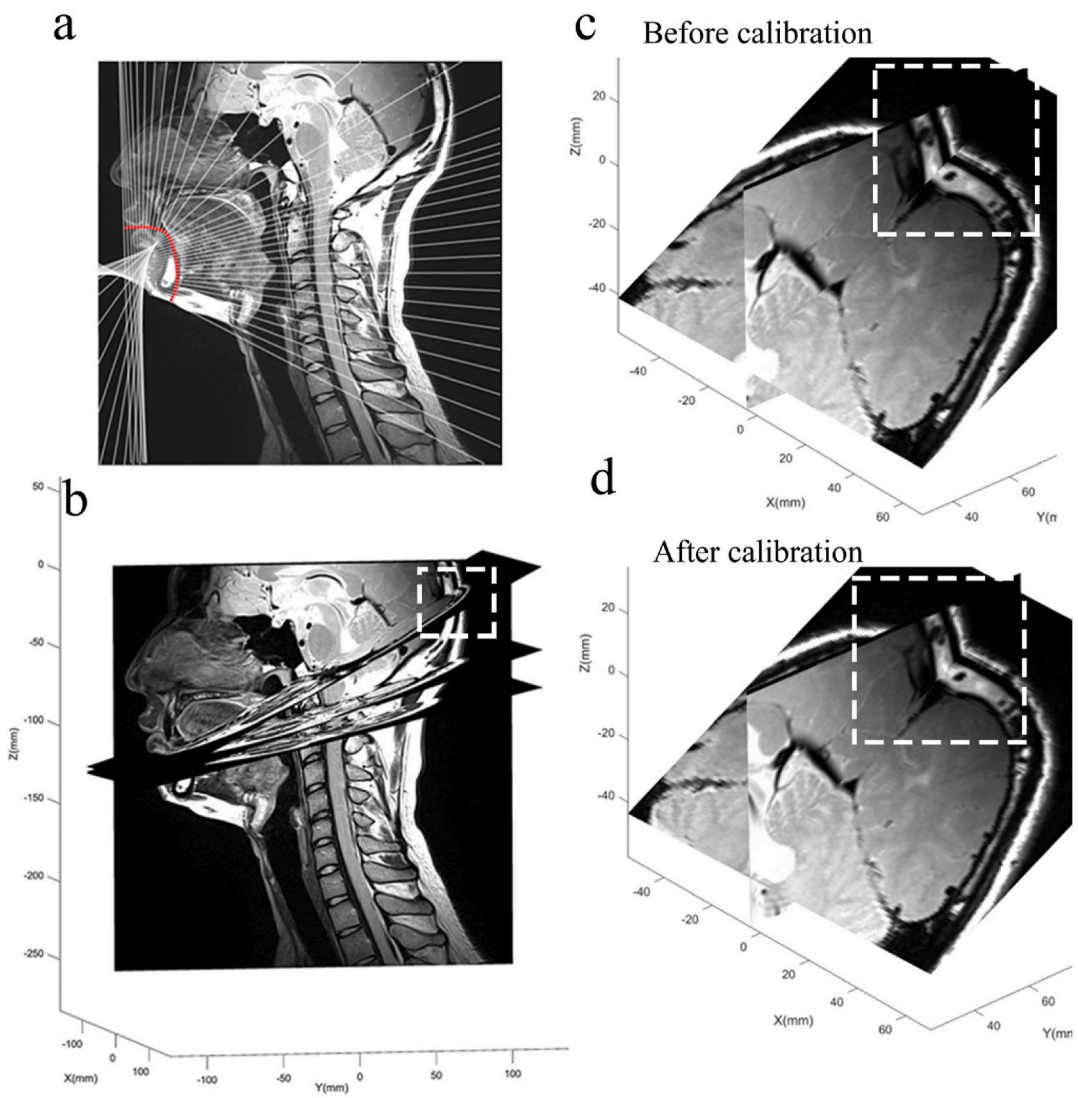


**Fig. 2.** The generation of multi-directional plane image sequence of the tongue. Each white line on the midsagittal plane in the subfigure (a) is a projection of the oblique section in the image sequence, perpendicular to the contour of the mandible shown by the red curve. The subfigure (b) is a 3D display of some reconstructed oblique cross-sectional images. The subfigures (c) and (d) show the results before and after calibration, respectively.

tissue may not yield optimal results. In this study, for each target tissue, we need to reconstruct one or more group of multiple parallel or non-parallel plane or curved images based on its structural characteristics, which are utilized for the reconstruction of the tissue structure. This approach allows us to extract as much tissue boundary information as possible from the reconstructed images, ultimately resulting in a more realistic 3D structure of the target tissue. For most head and heck tissues, a suitable set of image sequences is usually enough to build a 3D structure. However, the tongue and soft palate require more image sequences to reconstruct their 3D structure. Although the sagittal plane images can clearly display some contours of the tongue or soft palate, they could not provide information on the lateral edge of the tongue or soft palate. In such a case, a group of non-parallel images perpendicular to the mid-sagittal plane, as well as curved surface images were needed to effectively show the lateral boundaries.

#### 2.1.1. Oblique cross-sectional plane image

Taking the construction of multi-directional plane image sequence of the tongue as an example, the following is the basic mathematical algorithm for obtaining multi-directional cross-sectional images:

Based on the characteristics of the target tissue, a reference curve C(s) should first be manually selected on the sagittal plane, as shown by the red line in Fig. 2a.

The reference curve $C(s)$ lies within the sagittal plane $x = x_i$, and is parameterized as:

$$C(s) = (x_i, y(s), z(s)) \tag{1}$$

where $s$ is the parameter the curve.

According to the required number $N$ of planar images, $N$ points are selected on the reference curve $P_n(s) = (x_i, y(s_n), z(s_n)), n = 1, 2, \cdots, N$.

A plane perpendicular to the sagittal plane is constructed, which passes through the point $P_n(s)$ and perpendicular to the reference curve. Therefore, the normal vector of the plane is the tangent vector of the curve $T(s)$ at the point $P_n(s)$, that is

$$T_n(s) = \frac{dC(s)}{ds} = \left(0, \frac{dy(s)}{ds}, \frac{dz(s)}{ds}\right)_{s=s_n} \tag{2}$$

Using $T_n(s)$ as the normal vector of the plane, we can obtain the plane equation passing through the point $P_n(s)$:

$$T_n(s) \bullet ((x, y, z) - (x_i, y(s_n), z(s_n))) = 0 \tag{3}$$

For all points $P_n$ on the curve, where $n = 1, 2, \cdots, N,$ repeating the above process generates a set of multi-directional sequence planes. The grayscale value of each pixel on each plane is obtained from the original 3D scan image based on the spatial coordinates of the point. In this way, the construction of the set of multi-directional sequence plane images is completed.

#### 2.1.2. Curved section image

For constructing the curved section image, a curve is drawn on a selected sagittal image based on the characteristics of the target tissue, as illustrated by the red line in Fig. 3. This curve is then projected parallelly onto all sagittal images $i$, where $i = 1, 2, \cdots, M$. The grayscale values of each pixel on the curved section are obtained from the original 3D scanned image at the spatial coordinates of the

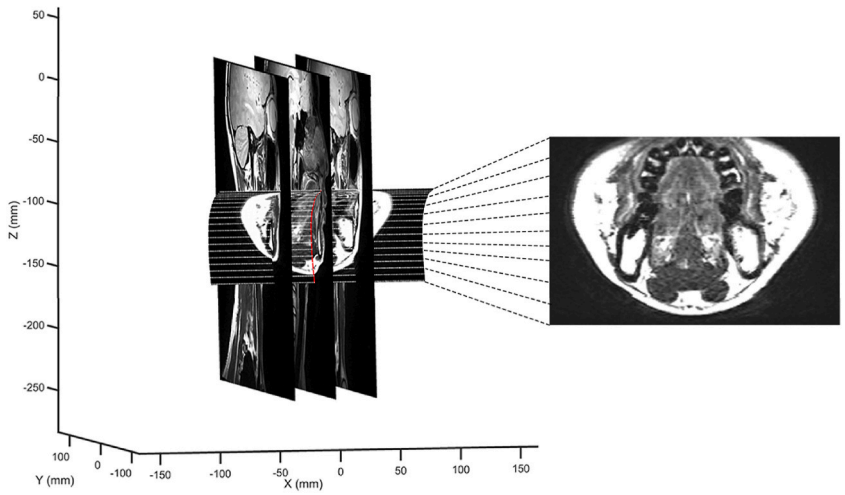


**Fig. 3.** The construction of a curved section image of the tongue. The left subfigure is a selected curved section image ranging from the tip of the tongue to the base of the tongue. The curved cross section is generated by translating the red curve in the direction perpendicular to plane of the sagittal image. The right subfigure is a planar image obtained by expanding the curved cross section shown in the left subfigure line by line, as shown by the dashed lines between the two subfigures.

respective points. In this way, the curved section image is constructed.

#### 2.1.3. Image calibration

After reconstructing multi-directional sectional images, these sections of different orientations will be calibrated. First, the midsagittal plane is used as the reference plane to determine the intersection line between the oblique sectional image and the midsagittal image. Next, the key feature points of the same anatomical structure along the intersection line are identified in both the midsagittal and oblique sectional images. Their alignment is then checked. If there is a discrepancy, the positional offset is calculated, and the oblique sectional image is adjusted by translating it according to the offset.

### 2.2. Boundary segmentation

The Matlab programs were written to segment the boundaries of tissues. For the boundary segmentation on 2D planar cross-sectional images, the spatial 3D coordinates of the extracted boundary points were stored as separate files. For the boundary segmentation of nasal airway and pharyngeal airway, we used a semi-automatic level set method, which handled changes in topology naturally, allowing the contour to split or merge, making it more efficient for segmentation of complex and irregular shapes [28]. Different from the boundary segmentation on the plane section image, the curved section image needs to be expanded into a plane image before the boundary segmentation operation was performed on the target tissue. After the boundary was segmented in the plane image formed by the expansion of the curved sectional image, the corresponding coordinate chart file was called to convert the index coordinates into spatial 3D coordinates.

### 2.3. Registration between multi-directional boundary curves

When more than one set of image sequences is needed to determine the boundary contours of a target tissue, the boundaries obtained from different image sets must be registered. Because the boundaries of the tongue or soft palate were from three image sequences, their boundary contours from different image sequences need to be registered. When registering the boundaries awaiting registration on other planes, the tissue boundary on the sagittal images remained fixed as a reference, and the boundaries in other planes should match the reference curve on the sagittal planes through different degrees of displacement or deformation.

The boundary contours of the tongue and soft palate were from three image sequences involving sagittal plane, oblique section and curved section, and the boundary curve on the oblique plane images or the curved surface images usually had no common intersection point with contour curves on the sagittal planes before registration. A two-step registration procedure was used to match the boundary curves segmented from three sets of images to build a high-precision 3D model of the tongue, as well as the soft palate, with complementary boundary contour curves. The first step was the initial registration of the boundaries on the planes of sagittal image and oblique image, and the second step was the registration of the initially registered boundaries on the planar images and the boundaries on the curved surface images.

### 2.4. Reconstruction of tissue 3D structure

The tissue boundaries obtained after above procedures can be represented by smooth spline interpolation functions. In the segmentation procedure, the sampling distance of the boundary points was less than one pixel, so the dense boundary points could ensure that the interpolated spline function accurately represented the original tissue boundary. The tissue contour was constructed by creating a surface that enclosed these boundary curves. Compared with B-spline curves, NURBS (Non-Uniform Rational B-Splines) curves are easier to control and can describe complex shapes, so we use NURBS functions to describe boundary curves. All boundary curves were input into NX-UG modeling software, through which the NURBS surface describing the tissue shape was generated [27].

### 2.5. Establishment of finite element model and numerical simulation

Meshing is a crucial step in finite element simulation, which often determines whether the calculation results converge. The constructed NURBS surface is naturally smooth, and can be used directly for high-quality meshing of finite element models. A one-way fluid-structure interaction computational model based on commercial software Ansys (ANSYS, Inc. Pennsylvania, USA) was used to simulate the closure of the upper airway during inspiration. The fluid domain was the entire upper airway, and the k-ε model was used to analyze the air flow in the airway. The solid domain included all soft tissue and bony tissue. The interface of fluid-structure interaction was the interface between the airway and the surrounding tissues. The posterior wall was set up as a rigid wall due to the bony structure of the vertebrae. The mechanical parameters of different tissues were given in Table 1. The pressure boundary conditions were set at the inlet and outlet of the airway. The nostrils were the inlet and the pressure was set to zero. The lower end of

**Table 1**
Young's modulus of the head and neck tissues.

| | Bone | Skin | Tongue | Soft palate | Muscle |
|---|---|---|---|---|---|
| Young's Modulus (Pa) | $1.72 \times 10^{10}$ [29] | $2 \times 10^{6}$ [29] | $6 \times 10^{3}$ [5] | $5 \times 10^{3}$ [5] | $1 \times 10^{4}$ [29] |

the airway was the outlet, and the pressure was set to a negative value, which can cause the airway to collapse and close.

In the finite element model, the solid domain used globally adaptive tetrahedral elements with a mesh size of 0.8 mm for the soft palate tissue, and 2.5 mm for others. The fluid domain employed adaptive tetrahedral elements with a mesh size of 0.5 mm. The computational model was steady-state, with a minimum of 5 iterations and a maximum of 100 iterations per time step. The convergence criterion was defined as the residual of the force being less than $1 \times 10^{-3}$. The critical closing pressure of the upper airway was defined as the pressure difference between the outlet and inlet of the airway that caused the soft palate or tongue to deform and thus contact the posterior wall of the airway. Since zero gauge pressure was set at the inlet of the airway, the airway outlet pressure when the soft palate or tongue body made contact with the posterior wall of the airway at a single element was used as the closing pressure in practical calculation. By progressively reducing the outlet pressure every $-25$ Pa, the transition from non-contact of the soft palate or tongue to initial contact of the posterior airway wall was observed.

## 3. Results

### 3.1. Reconstruction of image sequences for constructing different target tissues

For each target tissue around the upper airway, the construction of image sequences from the 3D MRI image for boundary segmentation was based on the structural characteristics of this specified tissue. Three sets of sequential images, including parallel sagittal plane images, non-parallel plane images, and curved surface images, were built for the reconstruction of the tongue. The reconstruction of image sequences with different orientations, but perpendicular to the sagittal plane, was based on the structure of the tongue on the sagittal sequence images. The planar sections with an arc-shaped opening, basically in the direction of tongue fibers, were oriented perpendicular to the reference curve along the posterior border of the mandible on the mid-sagittal plane. These multi-directional image planes transitioned gradually from the coronal plane to the axial plane as shown in Fig. 2. The structures of the tip, lateral sides, and base of the tongue were still not well reflected by these sectional images. The constructed curved surface images compensated for these shortcomings. Due to the non-planar nature of curved surface images, they could connect these regions in a single curved surface image. The curved surface image, which was perpendicular to the sagittal plane, was determined by the tongue midline or its vicinity on the mid-sagittal plane that connected the tongue tip region and tongue base region (Fig. 3). All curved surface images perpendicular to the sagittal plane could be unfolded into planar images without distortion, as shown in Fig. 3, which facilitated the extraction of tissue boundary information on the curved surface images. Then the coordinates of the boundary points

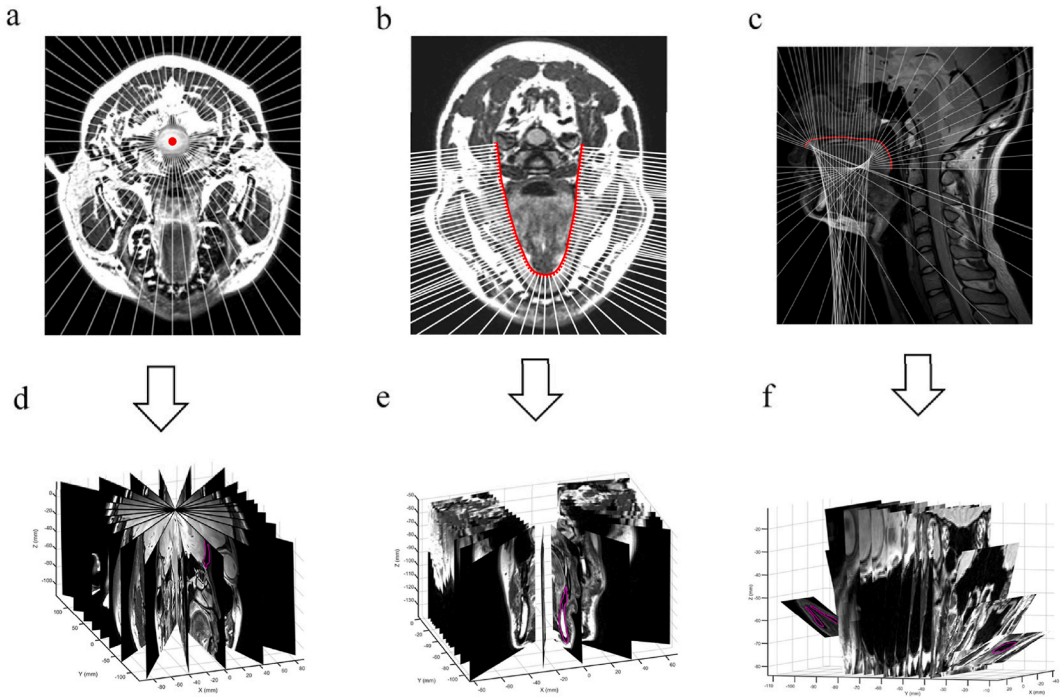


**Fig. 4.** The generation of multi-directional plane image sequences of different tissues. Subfigures (a), (b), and (c) are for the generation of the image sequences of the skull, mandible, and airway, respectively. The sequential images of the skull in (a) follow the white lines and are perpendicular to the plane of the axial image. The sequential images of the mandible in (b) follow the white lines and are perpendicular to both the U-shaped red reference curve and the plane of the axial image. The sequential images of the airway in (c) follow the white lines and perpendicular to the sagittal plane of the image. Subfigures (d), (e), and (f) are the 3D displays of some reconstructed oblique cross-section images corresponding (a), (b), and (c), respectively, and the contours of target tissues are represented by purple curves.

segmented on the expanded plane image were converted to the coordinates on the original spatial position of the curved surface image.

The generation of three sets of multi-directional planar sectional images and curved surface images for the boundary contour segmentation of the soft palate was similar to that for tongue, including parallel sagittal plane images, arc-shaped open plane images, and curved surface images connecting the tip of uvula and the hard palate.

For each of the other structures, only one set of multi-directional planar images was needed to reconstruct the 3D structure. The planar images used to construct the nasal airway were basically perpendicular to the direction of the air flow (Fig. 4c and f). The corresponding multi-directional planar images for the skull (Fig. 4a and d), mandible (Fig. 4b and e), hyoid bone, and cricothyroid cartilage, were constructed based on their anatomical characteristics.

### 3.2. Registration of boundary curves on different image sequences

The boundaries of the tongue and soft palate were composed of their boundaries on sagittal plane images, multi-directional planar images, and curved surface images. A nonlinear registration method was proposed to calibrate the boundary curves obtained by segmentation on different image sequences, which included two steps. In the first step of the registration process, the position of the points awaiting registration in the boundary on the oblique section image and the position of the target points in the reference boundary on the sagittal image were determined. The two points awaiting registration were the intersections of the boundary curves on the oblique image and the sagittal image plane, and the two target points were the intersections of the boundary curves on the sagittal image and the oblique image plane which were given by equation (4) and equation (5), respectively.

$$C_i(t) \cap \alpha_j = P_{ijk} \tag{4}$$

$$D_j(t) \cap \beta_i = Q_{ijk} \tag{5}$$

where $C_i(t)$ was the boundary curve on the $i$-th oblique image plane $\beta_i$, $P_{ijk}$, k = 1, 2, was the point awaiting registration, $D_j(t)$ was the reference curve on the $j$-th sagittal image $\alpha_j$, $Q_{ijk}$ was the target point, $i$ was from 1 to the total number of the oblique plane images, and $j$ was from 1 to the total number of the sagittal images, $t \in (0, 1)$ was the curve parameter. A displacement function $d(t)$, which regulated the displacement that each point in the boundary awaiting registration should move. According to the distance between the point awaiting registration and the corresponding target point, the displacement function can be given by nonlinear interpolation of the distance. Then, the boundary curve awaiting registration was shifted or deformed to the position of the registered point according to the displacement function. The processes were shown as follows

$$\begin{cases} Q_{ijkx} - P_{ijkx} = d_{ix}(\alpha_j, k) \\ Q_{ijky} - P_{ijky} = d_{iy}(\alpha_j, k) \\ Q_{ijkz} - P_{ijkz} = d_{iz}(\alpha_j, k) \end{cases} \xrightarrow{interpolation} \begin{cases} d_{ix}(t) \\ d_{iy}(t) \\ d_{iz}(t) \end{cases} \xrightarrow{displacement} \begin{cases} G_{ix}(t) = C_{ix}(t) + d_{ix}(t) \\ G_{iy}(t) = C_{iy}(t) + d_{iy}(t) \\ G_{iz}(t) = C_{iz}(t) + d_{iz}(t) \end{cases} \tag{6}$$

where $d_i(t)$ was the displacement function of each point on the curve $C_i(t)$ on the oblique image plane $\beta_i$ obtained by spline interpolation, $G_i(t)$ was the boundary curve after registration on the image plane $\beta_i$, the subscripts $x$, $y$, $z$ represented the three components

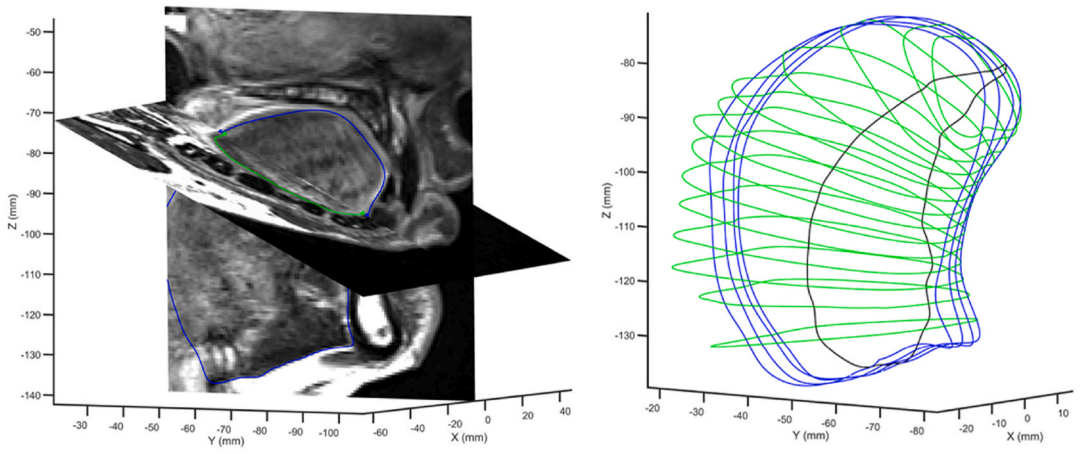


**Fig. 5.** The registration of the tongue boundary curves. In the left subfigure, the green boundary curve of the tongue located on the plane of the oblique section image is the curve awaiting registration, and the blue curve located on the sagittal image is the reference curve. The point awaiting registration marked by a green spot determined by Eq. (4) is the intersection point between the green boundary curve and the sagittal image, and the target point marked by a blue spot given by Eq. (5) is the intersection point of the blue boundary curve and the oblique section image. In the right subfigure, these green lines are the boundary curves of the tongue muscle on the oblique section images, the blue lines are the boundary curves of the tongue muscle on the sagittal planes, and the black line is the boundary contour of the tongue on the curved section image. These tongue boundary curves segmented from images in different directions have precise intersection points after the two-step registration.

of the coordinates in the Cartesian coordinate system.

The procedures of the second step of the registration were similar to the first step. The resulted boundary curves determined in the first step registration were the reference boundaries now. The intersections between the boundaries on the curved images and the oblique and sagittal plane images were the points awaiting registration, and the intersections between the reference boundaries on oblique and sagittal images and the curved image surfaces were the target points. Thus, a displacement function was constructed based on the distance between the points awaiting registration and the target points. Then, each point of the boundaries on the curved image surfaces was moved accordingly based on the displacement function and the boundaries on the curved image surfaces were registered. Through the above two-step registration method, the boundary curves of the tongue (Fig. 5) and soft palate in different image planes were effectively registered.

### 3.3. Construction of the 3D head and neck model

After registration, each boundary point of the tissue had its corresponding precise coordinates in the machine coordinate system, we could construct the 3D structure for any given tissue separately, and then assembled these separately constructed tissues together to form a 3D model of the entire head and neck. The common surface between adjacent tissues were formed by Boolean operations.

As an example, we compared the 3D structure of the tongue muscle reconstructed using our method of multi-directional non-parallel image sequences with the commonly used method based on parallel images obtained by scanning in one direction. Fig. 6 shows the reconstruction results using the multi-directional image sequences in our method (left) and the parallel sagittal image sequences in the commonly used voxel stacking method [30] (right). As can be seen from Fig. 6, the tongue body obtained by using only the tongue boundaries segmented from sagittal plane images is incomplete, showing the obvious absence of tissue on both sides.

Fig. 7 shows the constructed 3D structure of airway, tongue, soft palate, mandible, hard palate, nasal cavity, epiglottis, cricothyroid cartilage, trachea, skull, skin, etc., based on multi-directional cross-sectional images. The adjacency or contact between the tissues was accurately represented by the model. It could be seen that the contact region between the tongue and the soft palate, and the contact region between the genioglossus muscle and the mandible were consistent with the real anatomy. The front of the tongue was connected to the lower part of the mandible, the posterior part of the base of the tongue was adjacent to the hyoid bone, and the dorsum of the tongue was close to the soft palate.

The constructed nasal cavity model included the nostrils, nasal valves, inferior, middle, and superior turbinates, allowing easy calculation of the cross-sectional area and volume of the nasal airway, which was essential for the evaluation of nasal obstruction.

The epiglottic cartilage was constructed, the lower end was connected to the cricoid cartilage, and the front end was connected to the hyoid bone through a ligament. The hyoid bone was located at the lower part of the tongue base, and was pulled by the oblique upward stylohyoid muscle and downward sternocleidomis muscle, and the front end was under the action of the geniohyoid muscle.

### 3.4. Finite element simulation of upper airway obstruction

As an application example, the constructed 3D head and neck model was used to simulate airway collapse, a major clinical feature of sleep-disordered breathing. Fig. 8 shows the airway collapse process simulated by the one-way fluid-structure interaction numerical model. The simulation results showed that the displacement of the soft palate and the tongue muscle towards the posterior wall of the airway was the main cause of airway obstruction. The critical closing pressure at the outlet of the upper airway, which was used to describe the difficulty of airway collapse, was predicted by numerical simulation and given in Fig. 8. The more negative the value, the less likely the airway is to close. The numerical results showed that the patient with OSA had less negative critical closing pressure compared to the normal subject, indicating that the airway is more prone to collapsing and closing. The predicted critical closing pressure values of the normal subject and OSA patient are consistent with the in vivo measurements [31,32].

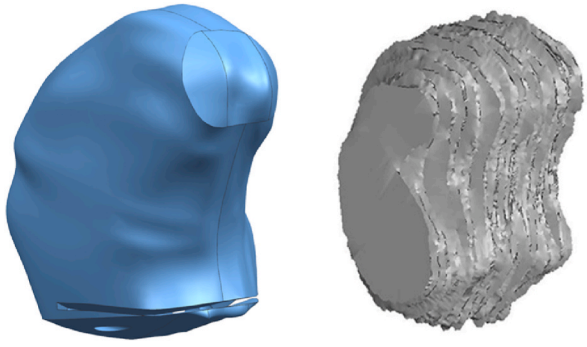

**Fig. 6.** A comparison between the tongue model constructed using the multi-directional boundary proposed in this paper and the model constructed using the voxel stacking method based solely on single-directional images.

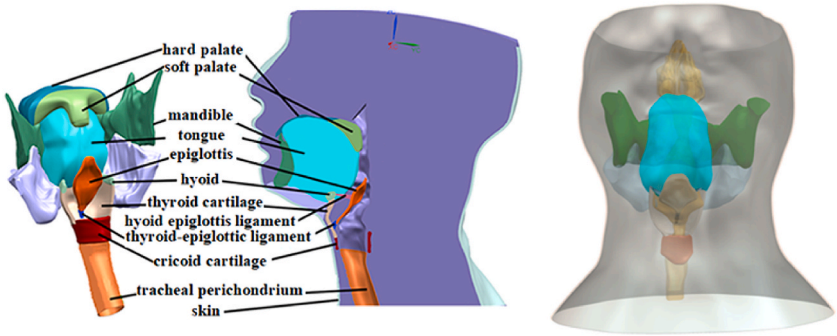


**Fig. 7.** The reconstructed 3D structures of head and neck tissues. The left panel shows the three-dimensional structure of the head and neck in the normal subject, while the right panel is a posterior view of the complete head and neck structure of the OSA patient.

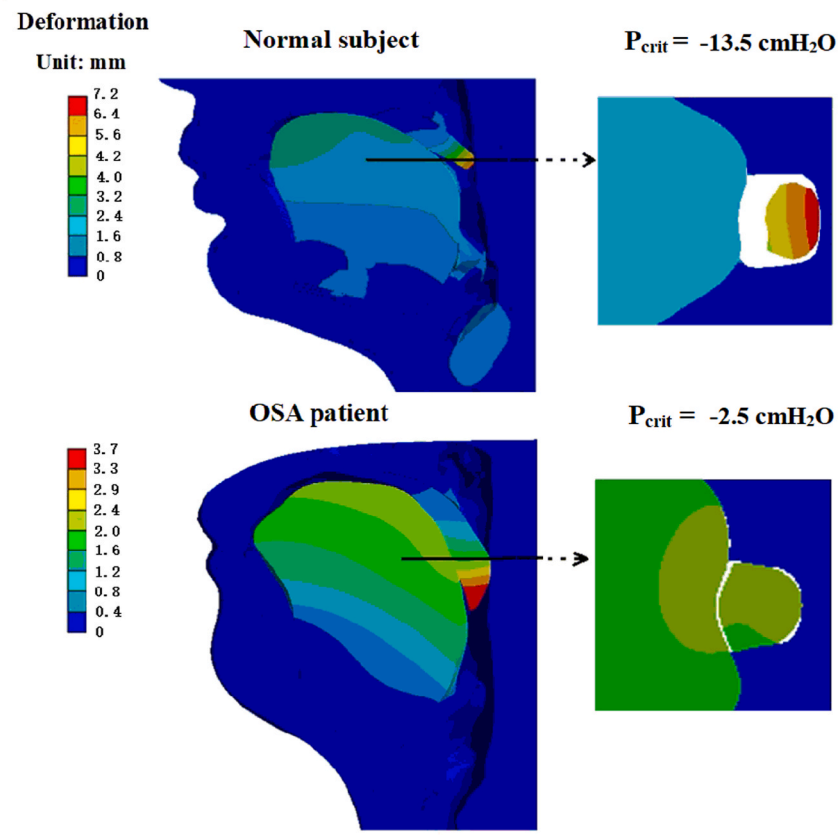


**Fig. 8.** The distribution of surrounding tissue deformation during airway collapse and closure (left), as well as the corresponding airway obstruction plane (right). $P_{crit}$ is the critical closing pressure at the outlet of the airway.

## 4. Discussion

This study proposes a comprehensive approach for 3D reconstruction of head and neck tissues, including multi-directional image reconstruction aligned with tissue structural features, nonlinear registration between complex boundary curves, and NURBS surface reconstruction for each tissue.

Even though artificial intelligence is highly anticipated in the field of image reconstruction, building complex 3D models of the head and neck remains a formidable challenge [33–35]. In this study, a novel reconstruction method of curved surface image is proposed, which makes up for the deficiency of plane cross-sectional images and provides complete information on the contours of the tongue and soft palate. To the best of our knowledge, this is the first study to utilize curved surface image for 3D reconstruction of tissue structures. Curved surface images are not restricted by planes and can represent multiple aspects of tissue boundaries on a single

surface.

It is inevitable to perform boundary registration between boundaries from multiple sets of image sequences in multiple directions. Unlike the registration between boundaries on two sets of planer image sequences, this study involves the complex registration between boundaries from multi-directional planer images and boundaries on curved surface images. The registration corrects the interpolation error when generating new image sequences as well as the boundary dislocations caused by partial volume effects, so that boundary curves obtained from different image sequences have the same intersection points. This boundary registration method provides a technical guarantee for accurate 3D structure reconstruction using multi-directional boundaries obtained on different image sequences.

Compared with the common modeling methods that only utilize the tissue boundary information obtained from single-directional scanning images, the multi-directional images and boundary registration approach proposed in this paper offers unique advantages, which can well meet the requirements of complex structure reconstruction by providing sufficient target tissue boundary information. Another advantage of our modeling approach is that it does not need to manually smooth the geometric model, since the NURBS surface enclosed by boundary curves is inherently a smooth structure. For the tongue geometry constructed by voxel stacking method as shown in Fig. 6, the rough surface of the tongue still requires further smoothing operations even if additional boundary information of other scanning directions is used. This smoothing operation may result in the loss of geometric features in the model.

The model we developed faithfully captures the features of the anatomical structure without any artificial smoothing. The geometric structures we construct are composed of boundary curves, and the surface of the tissue is precisely aligned with these boundaries. The accuracy of the geometric model is directly inherited from the precision of the boundary segmentation curves. The soft tissues and osseous tissues of the oropharynx have the correct connection mode and adjacent relationship according to the anatomical structure, and the tissues with different functions are distinguished and established separately.

The 3D model of the head and neck has a wide range of applications, not only for the evaluation of physiological functions such as breathing, swallowing and vocalization, and the planning of head and neck surgery [36,37], but also for the production of in vitro 3D experimental models [38]. The NURBS model can be seamlessly integrated into finite element analysis calculations, enhancing the potential of the head and neck geometric model we have built to be used in a wider range of simulation analyses [39,40]. In the article, we presented a simulation application based on this model as an example. The reason for choosing this particular simulation is that airway collapse involves complex factors, including complex anatomy of the head and neck, as well as complex calculation process for fluid-structure interaction. These aspects collectively impose strict requirements on the quality of the geometric model.

The constructed numerical model successfully simulated the airway collapse process and reasonably predicted the critical closing pressure of the airway, which is an important physiological parameter for measuring upper airway closure [41]. Currently, there is still a lack of comprehensive fluid-structure interaction models for the head and neck region to simulate airway collapse process [42]. Our simulation results provide comprehensive information regarding the deformation of various anatomical structures, including the tongue muscle, soft palate, airway wall, and epiglottis. The numerical simulation results show that the displacement of tongue and soft palate towards the posterior airway wall under the negative pressure of inspirations is the main factor leading to airway collapse and closure. The predicted critical airway closing pressure for obstructing the narrow upper airway in the OSA patient is significantly higher (i.e., the absolute value of negative pressure was smaller) than in the normal subject, which is consistent with clinical observations. Our results show that the comprehensive head and neck model developed in this study can provide a good technical basis for studying the mechanical mechanisms of airway collapse.

A limitation of this study is the exclusion of the 3D reconstruction of vertebrae. This is due to the fact that MRI images provide a lower resolution of vertebrae compared to CT images, and thus vertebral reconstructions usually rely on CT imaging. However, the method used to generate multi-directional image sequences is still applicable to the reconstruction of vertebrae. Our numerical simulation model of upper airway collapse does not include the vertebral structure, but has no significant impact on the simulation results because the posterior wall of the upper airway, which is mainly composed of vertebrae, is generally considered to be an undeformable rigid wall during breathing and is therefore not affected by the structural details of the vertebrae in the finite element model.

## 5. Conclusions

The method we developed for constructing multi-directional image sequences based on tissue characteristics can be effectively used to identify detailed contours of complex head and neck tissues. The nonlinear registration strategy established in this study can successfully match the boundaries segmented from plane and curved surface images with different orientations. The 3D model constructed based on the NURBS surface of the tissue contours can accurately characterize the realistic anatomical structure of the head and neck, which can be directly used to simulate the closure of the upper airway using the fluid-structure interaction method.

## CRediT authorship contribution statement

**Huahui Xiong:** Writing – review & editing, Writing – original draft, Validation, Methodology, Investigation, Funding acquisition, Formal analysis, Data curation, Conceptualization. **Hui Tong:** Writing – review & editing, Investigation, Formal analysis, Data curation. **Yuhang Tian:** Writing – review & editing, Investigation, Formal analysis, Data curation. **Changjin Ji:** Writing – review & editing, Investigation, Formal analysis. **Xiaoqing Huang:** Writing – review & editing, Investigation, Formal analysis. **Yaqi Huang:** Writing – review & editing, Supervision, Methodology, Investigation, Formal analysis, Conceptualization.

## Ethics statement

This study adhered to the principles of the Declaration of Helsinki and was approved by the Ethics Committee of Capital Medical University (approval number 2022SY073; approval date 2022.03.04). Written informed consent was obtained from all subjects to participate in the study and to publish the data.

## Data availability statement

Data used to support the findings is available upon request.

## Declaration of competing interest

The authors declare that they have no known competing financial interests or personal relationships that could have appeared to influence the work reported in this paper.

## Acknowledgements

This work was supported by grants from the Scientific Research Common Program of Beijing Municipal Commission of Education, China (KM201810025014).

## References

[1] X. Luo, K. Mori, T.M. Peters, Advanced endoscopic navigation: surgical big data, methodology, and applications, Annu. Rev. Biomed. Eng. 20 (2018) 221–251, https://doi.org/10.1146/annurev-bioeng-062117-120917.
[2] D.S. Shenaq, E. Matros, Virtual planning and navigational technology in reconstructive surgery, J. Surg. Oncol. 118 (2018) 845–852, https://doi.org/10.1002/jso.25255.
[3] J. Chmiel, K.P. Malinowski, K.M. Ksiazek, G. Wnuk, J. Dradrach, K. Proniewska, L. Partyka, K. Rosenfield, P. Musialek, Three-dimensional reconstruction of conventional catheter angiography-identified coronary artery aneurysms and ectasias, Am. J. Cardiol. 28 (2021) 623–626, https://doi.org/10.5603/CJ.a2021.0038.
[4] O. Tepper, D. Hirsch, J. Levine, E. Garfein, The new age of three-dimensional virtual surgical planning in reconstructive plastic surgery, Plast. Reconstr. Surg. 130 (2012) 192–194, https://doi.org/10.1097/PRS.0b013e318254fbf6.
[5] Y. Huang, A. Malhotra, D.P. White, Computational simulation of human upper airway collapse using a pressure-/state-dependent model of genioglossal muscle contraction under laminar flow conditions, J. Appl. Physiol. 99 (2005) 1138–1148, https://doi.org/10.1152/japplphysiol.00668.2004.
[6] A. Pugachev, M. Arnold, S. Burgmann, U. Janoske, Á. Bicsák, D. Abel, J. Linssen, L. Bonitz, Application of patient-specific simulation workflow for obstructive sleep apnea diagnosis and treatment with a mandibular advancement device, Int. J. Numer. Method. Biomed. Eng. 36 (2020) e3350, https://doi.org/10.1002/cnm.3350.
[7] M. Zhao, T. Barber, P.A. Cistulli, K. Sutherland, G. Rosengarten, Simulation of upper airway occlusion without and with mandibular advancement in obstructive sleep apnea using fluid-structure interaction, J. Biomech. 46 (2013) 2586–2592, https://doi.org/10.1016/j.jbiomech.2013.08.010.
[8] G. Mylavarapu, E. Gutmark, S. Shott, R. Fleck, M. Mahmoud, K. McConnell, R. Szczesniak, M.M. Hossain, G. Huang, D.G. Tadesse, C.L. Schuler, S. Khosla, R. Amin, Predicting critical closing pressure in children with obstructive sleep apnea using fluid-structure interaction, J. Appl. Physiol. 131 (2021) 1629–1639, https://doi.org/10.1152/japplphysiol.00694.2020.
[9] H.M. Beni, H. Mortazavi, M.S. Islam, Biomedical and biophysical limits to mathematical modeling of pulmonary system mechanics: a scoping review on aerosol and drug delivery, Biomech. Model. Mechan. 21 (2021) 79–87, https://doi.org/10.1007/s10237-021-01531-8.
[10] S. Buchaillard, M. Brix, P. Perrier, Y. Payan, Simulations of the consequences of tongue surgery on tongue mobility: implications for speech production in post-surgery conditions, Int. J. Med. Robot. Comp. 3 (2007) 252–261, https://doi.org/10.1002/rcs.142.
[11] J. Ohta, S. Ishida, T. Kawase, Y. Katori, Y. Imai, A computational fluid dynamics simulation of liquid swallowing by impaired pharyngeal motion: bolus pathway and pharyngeal residue, Am. J. Physiol. Gastrointest. Liver Physiol. 317 (2019) 784–792, https://doi.org/10.1152/ajpgi.00082.2019.
[12] P. Anderson, S. Fels, I. Stavness, W.G. Pearson, B. Gick, Intravelar and extravelar portions of soft palate muscles in velic constrictions: a three-dimensional modeling study, J. Speech. Lang. Hear. R. 62 (2019) 802–814, https://doi.org/10.1044/2018_JSLHR-S-17-0247.
[13] H. Fujita, Y. Uchiyama, T. Nakagawa, etal, Computer-aided diagnosis: the emerging of three CAD systems induced by Japanese health care needs, Comput. Meth. Prog. Bio. 92 (2008) 238–248, https://doi.org/10.1016/j.cmpb.2008.04.003.
[14] Y. Huang, G. Hu, C. Ji, H. Xiong, Glass-cutting medical images via a mechanical image segmentation method based on crack propagation, Nat. Commun. 11 (2020) 5669, https://doi.org/10.1038/s41467-020-19392-7.
[15] Z. Akkus, A. Galimzianova, A. Hoogi, D.L. Rubin, B.J. Erickson, Deep learning for brain MRI segmentation: state of the art and future directions, J. Digit. Imaging. 30 (2017) 449–459, https://doi.org/10.1007/s10278-017-9983-4.
[16] J. Lee, J. Woo, F. Xing, E.Z. Murano, M. Stone, J.L. Prince, Semi-automatic segmentation for 3D motion analysis of the tongue with dynamic MRI, Comput. Med. Imag. Grap. 38 (2014) 714–724, https://doi.org/10.1016/j.compmedimag.2014.07.004.
[17] H. Chen, S. Fels, T. Pang, L. Tsou, F.R. de Almeida, A.A. Lowe, Three-dimensional reconstruction of soft palate modeling from subject-specific magnetic resonance imaging data, Sleep Breath. 16 (2012) 1113–1119, https://doi.org/10.1007/s11325-011-0610-1.
[18] A. Bijar, P.Y. Rohan, P. Perrier, Y. Payan, Atlas-based automatic generation of subject-specific finite element tongue meshes, Ann. Biomed. Eng. 44 (2016) 16–34, https://doi.org/10.1007/s10439-015-1497-y.
[19] J.P. Pelteret, B.D. Reddy, Computational model of soft tissues in the human upper airway, Int. J. Numer. Method. Biomed. Eng. 28 (2012) 111–132, https://doi.org/10.1002/cnm.1487.
[20] H. Liu, V.E. Prot, B.H. Skallerud, Soft palate muscle activation: a modeling approach for improved understanding of obstructive sleep apnea, Biomech. Model. Mechanobiol. 18 (2019) 531–546, https://doi.org/10.1007/s10237-018-1100-1.
[21] K.H. Chang, Product Design Modeling Using CAD/CAE, first ed., Academic Press, Oxford, 2014, pp. 1–35.
[22] T. Miyazaki, Y. Hotta, J. Kunii, S. Kuriyama, Y. Tamaki, A review of dental CAD/CAM: current status and future perspectives from 20 years of experience, Dent. Mater. J. 28 (2009) 44–56, https://doi.org/10.4012/dmj.28.44.
[23] N. Yang, Z. Quan, D. Zhang, Y. Tian, Multi-morphology transition hybridization CAD design of minimal surface porous structures for use in tissue engineering, Comput. Aided Des. 56 (2014) 11–21, https://doi.org/10.1016/j.cad.2014.06.006.
[24] S.K. Kim, Y. Na, J.I. Kim, S.K. Chung, Patient specific CFD models of nasal airflow: overview of methods and challenges, J. Biomech. 46 (2013) 299–306, https://doi.org/10.1016/j.jbiomech.2012.11.022.

[25] N. Vukašinović, J. Duhovnik, Advanced CAD Modeling: Explicit, Parametric, Free-form CAD and Re-engineering, first ed., Springer International Publishing, 2019, pp. 1–64.
[26] T. Nagaoka, S. Watanabe, Voxel-based variable posture models of human anatomy, Proc. IEEE 97 (2009) 2015–2025, https://doi.org/10.1093/brain/awu203.
[27] H. Xiong, X. Huang, Y. Li, J. Li, J. Xian, Y. Huang, A method for accurate reconstructions of the upper airway using magnetic resonance images, PLoS One 10 (2015) e0130186, https://doi.org/10.1371/journal.pone.0130186.
[28] C. Li, C. Xu, C. Gui, M.D. Fox, Distance regularized level set evolution and its application to image segmentation, IEEE Trans. Image Process. 19 (2010) 3243–3254, https://doi.org/10.1109/TIP.2010.2069690.
[29] Y. An, C. Ji, Y. Li, J. Wang, X. Zhang, Y. Huang, In vivo measurements of human neck skin elasticity using MRI and finite element modeling, Med. Phys. 44 (2017) 1402–1407, https://doi.org/10.1002/mp.12154.
[30] Z. Li, M. Oskarsson, A. Heyden, Detailed 3D human body reconstruction from multi-view images combining voxel super-resolution and learned implicit representation, Appl. Intell. 52 (2022) 6739–6759, https://doi.org/10.1007/s10489-021-02783-8.
[31] I.C. Gleadhill, A.R. Schwartz, N. Schubert, R.A. Wise, S. Permutt, P.L. Smith, Upper airway collapsibility in snorers and in patients with obstructive hypopnea and apnea, Am. Rev. Respir. Dis. 143 (1991) 1300–1303, https://doi.org/10.1164/ajrccm/143.6.1300.
[32] E. Kazemeini, E. Van de Perck, M. Dieltjens, M. Willemen, J. Verbraecken, S. Op de Beeck, O.M. Vanderveken, Critical to know pcrit: a review on pharyngeal critical closing pressure in obstructive sleep apnea, Front. Neurol. 13 (2022) 775709, https://doi.org/10.3389/fneur.2022.775709.
[33] J.T.S. Phang, K.H. Lim, R.C.W. Chiong, A review of three dimensional reconstruction techniques, Multimed. Tools. Appl. 80 (2021) 17879–17891, https://doi.org/10.1007/s11042-021-10605-9.
[34] J. Minnema, A. Ernst, M. van Eijnatten, R. Pauwels, T. Forouzanfar, K.J. Batenburg, J. Wolff, A review on the application of deep learning for CT reconstruction, bone segmentation and surgical planning in oral and maxillofacial surgery, Dentomaxillofac, Radiol. 51 (2022) 20210437, https://doi.org/10.1259/dmfr.20210437.
[35] W. Zhu, Y. Huang, L. Zeng, X. Chen, Y. Liu, Z. Qian, N. Du, W. Fan, X. Xie, AnatomyNet: deep learning for fast and fully automated whole-volume segmentation of head and neck anatomy, Med. Phys. 46 (2019) 576–589, https://doi.org/10.1002/mp.13300.
[36] S.R. Moisik, B. Gick, The quantal larynx: the stable regions of laryngeal biomechanics and implications for speech production. J. Speech lang, Hear. Res. 60 (2017) 540–560, https://doi.org/10.1044/2016_JSLHR-S-16-0019.
[37] A. Ho, R. Affoo, N. Rogus-Pulia, M. Nicosia, Y. Inamoto, E. Saitoh, S. Green, S. Fels, Inferring the effects of saliva on liquid bolus flow using computer simulation, Comput. Biol. Med. 89 (2017) 304–313, https://doi.org/10.1016/j.compbiomed.2017.07.014.
[38] H. Wang, H. Wu, C. Ji, M. Wang, H. Xiong, X. Huang, T. Fan, S. Gao, Y. Huang, Mechanical mechanism to induce inspiratory flow limitation in obstructive sleep apnea patients revealed from in-vitro studies, J. Biomech. 146 (2023) 111409, https://doi.org/10.1016/j.jbiomech.2022.111409.
[39] G. Legrain, A NURBS enhanced extended finite element approach for unfitted CAD analysis, Comput. Mech. 52 (2013) 913–929, https://doi.org/10.1007/s00466-013-0854-7.
[40] M. Safdari, A.R. Najafi, N.R. Sottos, P.H. Geubelle, A NURBS-based generalized finite element scheme for 3D simulation of heterogeneous materials, J. Comput. Phys. 318 (2016) 373–390, https://doi.org/10.1016/j.jcp.2016.05.004.
[41] P.J. Hartfield, J. Janczy, A. Sharma, H.A. Newsome, R.A. Sparapani, J.S. Rhee, B.T. Woodson, G.J.M. Garcia, Anatomical determinants of upper airway collapsibility in obstructive sleep apnea: a systematic review and meta-analysis, Sleep Med. Rev. 68 (2023) 101741, https://doi.org/10.1016/j.smrv.2022.101741.
[42] W.M. Faizal, N.N.N. Ghazali, C.Y. Khor, Irfan Anjum Badruddin, M.Z. Zainon, Aznijar Ahmad Yazid, Norliza Binti Ibrahim, Roziana Mohd Razi, Computational fluid dynamics modelling of human upper airway: a review, Comput. Methods. Programs, Biomed 196 (2020) 105627, https://doi.org/10.1016/j.cmpb.2020.105627.